

Finite T electroweak phase transition on the lattice[†]K. Rummukainen^{a*}^aIndiana University, Department of Physics, Swain Hall-West 117, Bloomington, IN 47405, USA

This talk reviews recent lattice results on the high T electroweak phase transition. A remarkably accurate picture emerges: a) the transition is of first order for $m_H \lesssim 80$ GeV and vanishes for larger m_H ; b) transition temperature, latent heat and interface tension are known, as well as c) the properties of the broken and symmetric phases. New developments in the sphaleron rate calculations are discussed.

1. INTRODUCTION

At high temperatures the spontaneously broken symmetry of the electroweak (EW) sector of the standard model is restored [1]. How this restoration occurs is crucial for understanding the effects of EW physics to the baryon number of the Universe, and for the viability of EW baryogenesis [2]. The essential questions are: what is the order of the transition, or is there only a smooth cross-over? What are the values of the transition temperature T_c , latent heat L , interface tension σ and the discontinuity of the Higgs condensate? Very important are also the properties of the phases close to T_c : the equation of state, screening lengths, and phase metastability ranges. For baryogenesis scenarios, a crucial quantity is the sphaleron rate, i.e. the rate of the baryon number fluctuation. These quantities are parametrized by the still unknown Higgs mass m_H (experimentally $m_H \gtrsim 64$ GeV). All of the questions above have been addressed with lattice simulations; and happily, more often than not, definite answers have been found.

Given the success of the EW perturbation theory at $T = 0$, it is natural to apply it at finite T : indeed, the effective potential has been calculated up to 2-loop level [3,4]. However, it has become clear that the perturbation theory in gauge theories at high T is intrinsically unreliable due to infrared divergences [5]. At low T the perturbative expansion is regulated by the large value of

the Higgs condensate v : the expansion parameter is $\sim g^2 T / [\pi m_W]$. When T increases, v becomes smaller, and in the symmetric phase the expansion cannot be controlled even with resummation techniques. Clearly, a non-perturbative approach is required.

In comparison with the QCD phase transition, until recently the finite T EW transition had not been extensively studied. Since the non-perturbative effects are expected to be mainly due to the SU(2) gauge fields, the studies have concentrated on the SU(2) gauge + Higgs model. A direct way to study the finite T physics is to perform 4D Euclidean lattice simulations; the standard formalism was set up almost a decade ago [6,7], but the first results close to the physical weak coupling parameter values were published only in 1992 [8]. The development of the dimensionally reduced 3 dimensional effective formalism, initiated in [9] and completed in [4,10], was an important milestone theoretically and especially for practical simulations. Until Lattice '95, Higgs mass ranges $m_H = 18\text{--}49$ GeV had been investigated with 4D simulations [11–13] and 35–80 GeV with the 3D formalism [9,14–16] (for earlier reviews, see [17–19]). In this conference new 4D results with $m_H \lesssim 102$ GeV were presented by the DESY group [20–22] and Y. Aoki [23], and 3D results with $m_H \leq 180$ GeV by Kajantie et al.[24,25], Karsch et al.[26,27], Gürtler et al.[28] and Philipsen et al.[29]. New studies of the sphaleron rate were reported by Tang and Smit [30].

*e-mail: kari@trek.physics.indiana.edu

Address after 9/96: Universität Bielefeld, Germany

[†]Review talk at LATTICE96, St. Louis, USA, June 1996

2. THE SU(2)-HIGGS MODEL

Since the essential physics of the EW phase transition is expected to arise from SU(2) gauge fields and the Higgs field, let us for the moment neglect SU(3) and U(1) components of the gauge fields and the fermions entirely. The SU(2)-Higgs Euclidean Lagrangian is

$$L = \frac{1}{4}F_{\mu\nu}^a F_{\mu\nu}^a + (D_\mu\phi)^\dagger (D_\mu\phi) - m^2\phi^\dagger\phi + \lambda(\phi^\dagger\phi)^2, \quad (1)$$

where $\phi = (\phi^+, \phi^0)$ is the Higgs doublet. In the following we discuss the derivation of the effective 3D action from (1).

2.1. 3D effective action: why and how

Because of the relatively small value of the coupling g , the EW theory at high temperatures has a very wide range of mass scales (\sim inverse screening lengths):

$$T \gg m_D \approx gT \gg g^2T, m_W(T), m_H(T). \quad (2)$$

For example, the simulations have shown that if $m_H \approx 60$ GeV, then $m_H(T_c) < 0.1T_c$. On an Euclidean finite T system the imaginary time is restricted to the interval $0 \leq \tau \leq 1/T$; thus, when this system is latticized, in order to avoid finite size effects the ratio of the spatial and temporal extents of the lattice should be at least $L_s/L_\tau \gtrsim 30$ –40. This is a very punishing requirement.

The extreme ‘flatness’ of the geometry already suggests that the essential features of the system might be described by an effective 3D theory. Because of the periodic boundary conditions, when the bosonic fields are expanded in Fourier modes the inverse propagator becomes $[\vec{k}^2 + m_0^2 + (2\pi nT)^2]$. If T is large compared to the other relevant mass scales of the system, the non-static Matsubara modes with $n = \pm 1, \pm 2, \dots$ acquire a heavy mass $2\pi nT$ and can be integrated over. What remains is an effective 3D theory of the static ($n = 0$) modes. If the original 4D theory has fermions, then, because of the antiperiodicity in τ , *all* fermionic modes become massive with $m = (2n + 1)\pi T$ and can be integrated over. The effect of the fermion fields is only to adjust the parameters of the effective 3D bosonic

theory. The derivation of the 3D effective theory, *dimensional reduction* (DR), introduced in [31], was fully developed for the EW theory in [4,10,32].

The integration over the non-static modes can be performed *perturbatively*. This is possible if

- $g^2, \lambda \ll 1$
- $T \gg m_Q(T_c)$, the relevant mass scales at T_c .

For the EW transition, these conditions are met when $30 \lesssim m_H \lesssim 240$ GeV: the lower bound comes from the requirement that $m_H(T)$, $m_W(T)$ must be $\ll T$ in the vicinity of T_c , and the upper bound from the fact that for large m_H the EW theory becomes strongly coupled. Note that there are no IR problems in the *derivation* of the effective action: the IR modes are inherently 3-dimensional and are not integrated over. Indeed, the effective theory retains all IR divergences of the original theory! Moreover, the perturbative DR does not require that the finite T perturbation theory should be applicable in general: the criterion for finite T perturbation theory to work is $g^2T/m_Q \ll 1$, which is not satisfied at high T .

Starting from eq. (1) the effective theory can be defined by the action $S_3[A_0^a(\vec{x}), A_i^a(\vec{x}), \phi(\vec{x})]$, a 3D SU(2) gauge + adjoint Higgs + fundamental Higgs theory, where the coefficients of the action depend on the original 4D action coefficients. The adjoint Higgs A_0 is the remnant of the time-like component of the 4D gauge field. This action was used in [9,14] to simulate $m_H = 35$ and 80 GeV systems. Further, for the EW theory, one observes that the Debye mass $m_D = \sqrt{5/6}gT$ is large, and the field A_0 can also be integrated over. The resulting action

$$S_3[A_i, \phi] = \int d^3x \left[\frac{1}{4}F_{ij}^a F_{ij}^a + (D_i\phi)^\dagger (D_i\phi) + m_3^2\phi^\dagger\phi + \lambda_3(\phi^\dagger\phi)^2 \right] \quad (3)$$

has been the ‘workhorse’ in all recent 3D simulations [24,28,26]. It is similar in form to the original 4D action (1); however, now the fields and couplings have dimensions $[\phi] = \text{GeV}^{1/2}$, $[g_3^2] = [\lambda_3] = \text{GeV}$. In [33] the action was further simplified to an O(4)-symmetric scalar theory by integrating over the gauge fields. However, this action failed to describe the phase transition

correctly, indicating the essential role of the magnetic sector of the gauge fields.

The theory is now uniquely fixed by three parameters, the gauge coupling g_3^2 and two dimensionless numbers

$$x \equiv \lambda_3/g_3^2, \quad y \equiv m_3^2(g_3^2)/(g_3^2)^2 \quad (4)$$

The action (3) is *superrenormalizable*: the couplings g_3^2 and λ_3 do not run (in $\overline{\text{MS}}$), and m_3^2 has only linear and log-divergences at 1- and 2-loop levels. This property makes the relation between lattice action and continuum parameters (4) particularly transparent, as discussed in section 2.3.

The action of form (3) can be derived already with 1-loop DR. However, to fully utilize the superrenormalizability better accuracy is required, and in [4,10,24] DR is performed with *Green's function matching*: one starts from a general 3D superrenormalizable action and matches all 2- and 4-point Green's functions to the static 4D Green's functions of the original theory. To cancel large logarithms (in $\overline{\text{MS}}$), the 4D couplings are run to scale $\mu = 4\pi T e^{-\gamma} \approx 7T$ by the standard 4D β functions. The matching is done to a consistent accuracy in g^2 , λ . The action (3) can provide the relative accuracy $\delta G/G \sim O(g^3)$. To go beyond this would require the inclusion of 6-dim. operators while giving up superrenormalizability. By calculating the effects of the excluded higher dimensional operators the accuracy of the effective action can be estimated [10]. By construction, the Green's function matching avoids the non-localities inherent in the standard integration and 'block transformation' -type approaches to effective actions [34].

The DR process provides us with the essential relations between the 3D and 4D parameters. There is a large class of 4D theories which map into the 3D SU(2)+Higgs theory. Since the fermions do not 'survive' DR, this class includes the 4D theory of SU(2) + Higgs + fermions and the minimal standard model (MSM), where the effect of U(1) gauge field can be estimated perturbatively. The mapping $(g_3^2, x, y) \leftrightarrow$ 4D parameters for these theories has been worked out in detail in [10]. Conversely, a single 3D simulation can yield physical results for the whole class of 4D theories. Recently DR has been worked out

for MSSM by several authors [35].

For the 4D SU(2)-Higgs theory the relation 4D \leftrightarrow 3D is [10,24]

$$g_3^2 = 0.44015T^* \quad (5)$$

$$x = -0.00550 + 0.12622h^2 \quad (6)$$

$$y = 0.39818 + 0.15545h^2 - 0.00190h^4 - 2.58088(m_H^*/T^*)^2, \quad (7)$$

where $h = m_H^*/m_W$, $m_W = 80.6 \text{ GeV}$ and

$$g = \frac{2}{3}, \quad \lambda = \frac{1}{8}g^2(m_H^*/m_W)^2 \quad (8)$$

(The authors of [26,28] use somewhat different conventions.) The notation m_H^* , T^* is used to remind that these are not the physical T or the pole m_H ; for the SU(2)-Higgs theory without fermions the difference is small. These parameters are used extensively to present the results of 3D simulations.

2.2. Lattice action in 4D

The lattice action is conventionally written as

$$\begin{aligned} S = & \beta_G \sum_{x; \mu < \nu} (1 - \frac{1}{2} \text{Tr } P_{x; \mu\nu}) \\ & - \beta_H \sum_{x; \mu} \frac{1}{2} \text{Tr } \Phi_x^\dagger U_{x; \mu} \Phi_{x+\hat{\mu}} \\ & + \sum_x \frac{1}{2} \text{Tr } \Phi_x^\dagger \Phi_x + \beta_R \sum_x [\frac{1}{2} \text{Tr } \Phi_x^\dagger \Phi_x - 1]^2 \end{aligned} \quad (9)$$

where $\Phi = R \times V$, $V \in \text{SU}(2)$, and $R^2 = \frac{1}{2} \text{Tr } \Phi^\dagger \Phi$. The Higgs field Φ has $\text{SU}(2)^{\text{gauge}} \otimes \text{SU}(2)^{\text{global}}$ symmetry.

The essential question is now the relation of the lattice parameters to continuum physics. In the 4D formalism this is done non-perturbatively, relying only on the measurements of physical quantities. This comes at a cost: simulations at $T = 0$ are needed in order to set the scale. At tree level, the relation is

$$\beta_G = 4/g^2 \quad (10)$$

$$(ma)^2 = (1 - 4\beta_H - 2\beta_R)/\beta_H \quad (11)$$

$$\lambda = 4\beta_R/\beta_H^2. \quad (12)$$

Strictly speaking, for the 4D SU(2)-Higgs the $a = 0$ limit cannot be reached because of triviality. The term "continuum limit" in this case

means reaching a region where the cut-off effects become negligible: physics remains invariant when moving along the renormalization group trajectories, or *constant physics curves* (CPC).

The most detailed scaling study so far has been performed by the DESY group [20] using lattices with $N_\tau = 1/(aT) = 2-5$. A practical way to determine CPCs is to use the transition itself as follows [12,20]:

(a) To be close to the desired physical point $g^2 \approx 0.5$, $m_H \approx 34 \text{ GeV}$, couplings $\beta_G = 8$, $\beta_R = 0.0003$ are chosen for $N_\tau = 2$ simulations. m_W is fixed to 80 GeV. The value of β_H is tuned until the transition coupling $\beta_{H,c}$ is found.

(b) Using these couplings one performs $T = 0$ ($N_\tau \gtrsim N_s$) simulations. Higgs and W masses and the static potential (Wilson loops) are measured; from the static potential the renormalized gauge coupling g_R^2 can be extracted. This also gives $\lambda_R \equiv g_R^2/8(m_H/m_W)^2$.

(c) Using the known continuum 1-loop RG-equations for β_G and β_R , one runs along CPC from $N_\tau \rightarrow N_\tau + 1$ ($a \rightarrow aN_\tau/(N_\tau + 1)$). The step (a) is then repeated with the new couplings.

Good scaling now means that dimensionless physical quantities g_R^2 , λ_R , T_c/m_W remain invariant. This is surprisingly well satisfied already when $N_\tau = 2 \rightarrow 3$, in strong contrast to QCD or even pure gauge $SU(N)$ phase transitions, where scaling violations are still seen at $N_\tau = 6$. Especially the $T = 0$ quantities g_R^2 and m_H/m_W do not show systematic a -dependence beyond the statistical errors. In this case $g_R^2 \approx 0.585$ and $m_H/m_W \approx 0.422$, close to the tree level value. The good scaling behaviour indicates that the modes constant in τ are the dominant ones.

In the physically allowed range $m_H \gtrsim 64 \text{ GeV}$, the inequality $T \gg m_H(T)$, $m_W(T)$ makes the 4D formalism very unwieldy. An appealing remedy for this is to use *asymmetric lattice spacings* $a_s = \xi a_\tau$. The kinetic part of eq. (9) splits into temporal and spatial parts with couplings β_G^τ , β_G^s and β_H^τ , β_H^s . The couplings are related to the asymmetry through relations $\beta_i^\tau/\beta_i^s = f_i(\xi)$. These have been evaluated perturbatively to order $O(g^2, \lambda)$ by requiring isotropy in the W and Higgs correlations [36]. In non-perturbative tests these relations were reproduced very accu-

rately [22].

2.3. Lattice action in 3D

The 3D $SU(2)$ -fundamental Higgs lattice action is similar in form to the 4D action in eq. (9), except now the indices are limited to values 1–3. The essential difference between the 4D and 3D formalisms becomes evident when we look at the derivation of the CPCs. The crucial point is the superrenormalizability of the 3D action (3): g_3^2 and λ_3 do not run, and $m_3^2(g_3^2)$ has only 1- and 2-loop divergences. Calculating the relevant diagrams both in the continuum and on the lattice one obtains the relations [10,24]

$$g_3^2 a = \frac{4}{\beta_G} \quad (13)$$

$$x = \frac{1}{4} \lambda_3 a \beta_G = \frac{\beta_R \beta_G}{\beta_H^2} \quad (14)$$

$$\begin{aligned} y &= \frac{\beta_G^2}{8} \left(\frac{1}{\beta_H} - 3 - \frac{2x\beta_H}{\beta_G} \right) + \frac{3\Sigma\beta_G}{32\pi} (1 + 4x) \\ &+ \frac{1}{16\pi^2} \left[\left(\frac{51}{16} + 9x - 12x^2 \right) \left(\ln \frac{3\beta_G}{2} + \zeta \right) \right. \\ &\left. + 5.0 + 5.2x \right]. \end{aligned} \quad (15)$$

Eq. (15) depends on several constants arising from lattice perturbation theory: $\Sigma = 3.17591$, $\zeta = 0.09$, and the two numbers 5.0 and 5.2, specific for $SU(2)$ -Higgs theory and calculated in [32].

For fixed continuum parameters (g_3^2, x, y) eqs. (13–15) define the CPC in the space of $(\beta_G, \beta_H, \beta_R)$ when lattice spacing a is varied. Also note that in 3D $\beta_G \propto 1/a$. In contrast to the 4D case the continuum limit is well defined in 3D. The equations above have relative accuracy $O(a^{-1})$, so that the relation continuum \leftrightarrow lattice becomes exact when $a \rightarrow 0$. However, in practice the finite a effects have been observed to be small.

The Bielefeld group [26,27] takes a different philosophy to 3D effective theories: they do not utilize the superrenormalizability of the 3D action, but consider that the most natural approach is to fix the cutoff scale to be of the same order of magnitude than the physical scales. While this introduces differences $\propto a$, the smallness of the finite a effects makes most of the results comparable to the $a \rightarrow 0$ results.

3. PHASE TRANSITION

3.1. Phase diagram

In previous Lattice meetings [18,17] results with m_H from 18 to 80 GeV were reported. The transition was seen to be quite strongly 1st order at small m_H , and to weaken rapidly with increasing m_H . When $m_H = 80$ GeV the resolution was not good enough to distinguish the order of the transition. Since this mass region is expected to be physically relevant, it is essential to clarify the situation at larger m_H .

An important point in understanding the phase structure is the observation that the EW theory does not have a true gauge invariant order parameter which would distinguish the symmetric and Higgs phases. Indeed, it has been shown analytically that in the SU(2)-Higgs lattice system where the Higgs length is fixed the Higgs and the confined phases are analytically connected [37] in the strong coupling regime; this was also observed in the early simulations [6,7].

A study of one-loop Schwinger-Dyson equations [38] argues in favour of the end of the 1st order transitions at $m_H \sim 100$ GeV, after which only a smooth cross-over remains. This is certainly consistent with the observations above. However, the result relies on the applicability of the perturbation theory, which is known to break down at $m_H \sim 80$ GeV. On the other hand, ϵ -expansion techniques [39] predict that a weak 1st order transition remains even with large m_H . Due to the lack of an order parameter, it is not likely that the 1st order transition turns into a line of 2nd order transitions.

The situation has been addressed by the recent 3D [25–27] and 4D [23] simulations, which indicate that the transition turns into a smooth cross-over at $m_H \approx 80$ GeV. Kajantie et al. [25] utilized the finite size behaviour of the $\phi^\dagger\phi$ susceptibility (in 3D notation):

$$\chi = g_3^2 V \langle (\phi^\dagger\phi - \langle \phi^\dagger\phi \rangle)^2 \rangle \quad (16)$$

where $\langle \phi^\dagger\phi \rangle / g_3^2 = \beta_G \beta_H \langle R^2 \rangle / 8 + \text{const.}$ and $V(g_3^2)^3 = (4N/\beta_G)^3$. For each V the temperature is adjusted until the maximum value of χ is found. According to the finite size scaling, in 1st order transitions $\chi_{\max} \propto V$, in 2nd or-

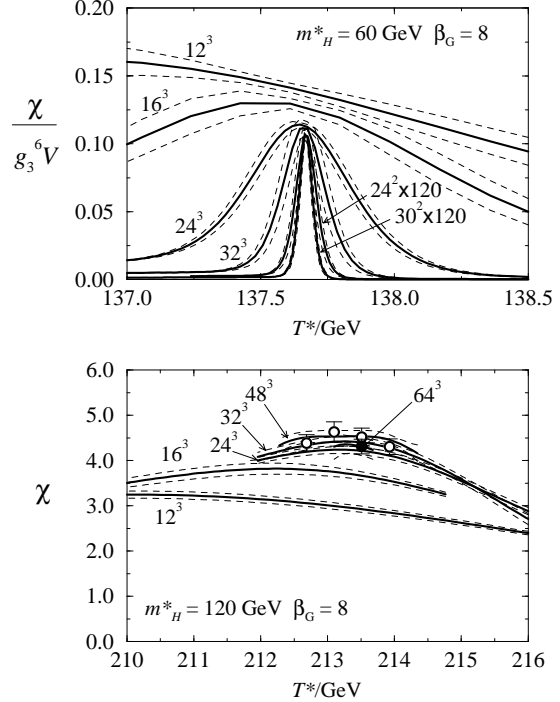


Figure 1. $\chi(T)$ for $m_H^* = 60$ and 120 GeV around the maximum [25] (Note the different y -axes!).

der transitions $\chi_{\max} \propto V^{\gamma/3}$, where γ is a critical exponent, and if there is no transition χ_{\max} approaches a constant value. In Fig.1 $\chi(T)$ is shown for $m_H^* = 60$ and 120 GeV. The difference is striking: the quantities χ_{\max}/V (60 GeV) and χ (120 GeV) approach constant values, consistent with a 1st order transition and no transition, respectively. χ_{\max} for $m_H^* = 35$ –180 GeV are plotted against V in Fig.2. Scaling is well satisfied: points with different β_G fall on the same curve. To emphasize the approach to the asymptotic V^1 , V^0 -lines, a simple mean field model has been fitted to the data; the results of the fits are shown as continuous curves.

Similar behaviour was reported by Y. Aoki [23], using 4D $m_H = 47$ –102 GeV simulations, and by the Bielefeld group [27], using $m_H = 60$ –100 GeV in 3D. Interestingly, also in finite T U(1)-Higgs theory an endpoint of the 1st order phase transitions has been observed [40].

A more detailed study of the properties of

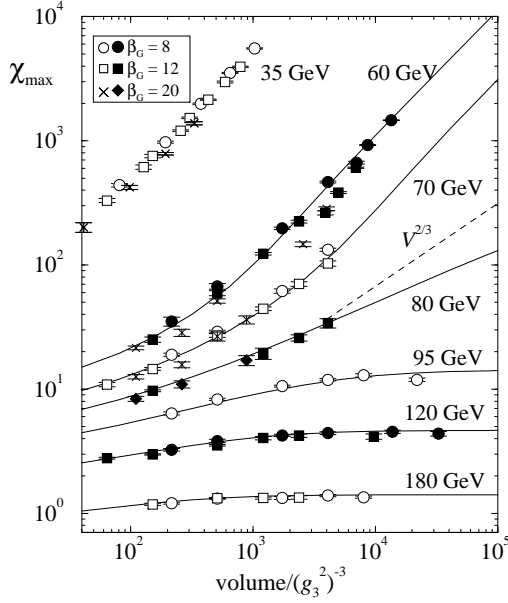


Figure 2. χ_{\max} for different m_H^* as a function of V . The continuous lines are mean field fits, the dashed line corresponds to the mean field critical exponent.

the critical point was performed in [27]. In the $m_H = 80$ GeV case $m_H(T)$ was measured around the transition in the symmetric and broken phases and fitted to the ansatz

$$m_H \propto |\beta_G - \beta_{G,c}|^\nu \quad (17)$$

(here β_G is adjusted while keeping β_H , β_R constant), with the result $\nu = 0.49(2)$ and $0.31(1)$ in the symmetric and broken phases, respectively. The different indices could indicate a tricritical nature for the endpoint; on the other hand, 80 GeV is likely not the exact value of $m_{H,c}$. Indeed, utilizing the analysis of the Lee-Yang zeroes for $m_H = 80$ and 100 GeV it was estimated that $m_{H,c} \approx 77$ GeV.

3.2. T_c and metastability

To accurately locate T_c both the finite size and finite lattice spacing effects have to be addressed. In 3D simulations, for fixed $\beta_G = 4/(g_3^2 a)$, x and V , one adjusts y in order to find the pseudocritical point (β_H and β_R are given by eqs. (14–15)). Through eqs. (5–7) this corresponds exactly to adjusting T^* while keeping m_H^* constant.

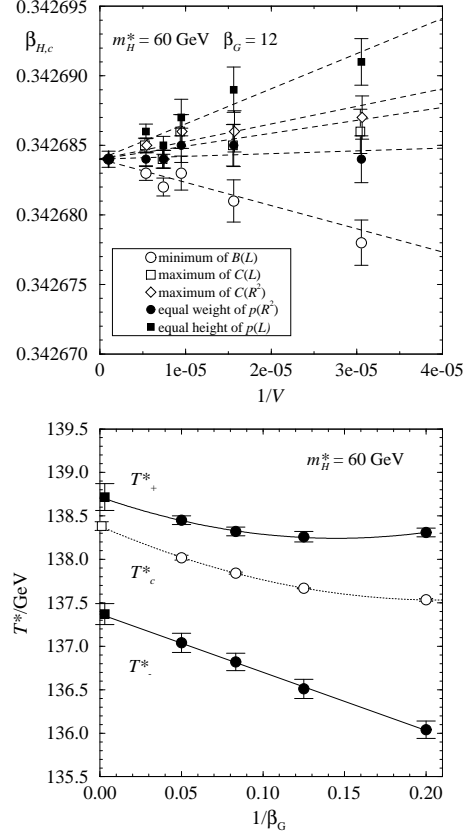


Figure 3. Top: the $V \rightarrow \infty$ extrapolation of the pseudocritical coupling $\beta_{H,c}$. Bottom: the continuum limit ($1/\beta_G = 0$) extrapolation of T_c (open symbols). Also shown here is the metastability range (filled symbols) [24].

With finite V , there are several non-equivalent methods to locate the pseudocritical point: the maximum of the order parameter susceptibility, the minimum of the Binder cumulant and the “equal weight” and “equal height” points of the order parameter distributions [24,28]. In the $V \rightarrow \infty$ limit these all extrapolate to the same value, as shown in top part of Fig. 3. Multicanonical simulations and histogram reweighting are commonly used in the analysis. This is repeated for 2–4 values of β_G while x is kept constant. The continuum limit is obtained by extrapolating in $1/\beta_G$. This is shown in Fig. 3 for $m_H^* = 60$ GeV; in this case the range in β_G -values (5–20) is so

Table 1

T_c^* and T_c for physical SU(2)+Higgs and physical SU(2)+Higgs+fermions -theories. $m_H^* = 35$ –70 is from [24], 72.18 from [28] (70 GeV in authors' notation). All units are in GeV.

m_H^*	35	60	70	72.18
T_c^*	92.64(7)	138.38(5)	154.5(1)	157.74(5)
$T_{c,\text{pert}}^*$	93.3	140.3	157.2	160.9
SU(2)+Higgs				
m_H	29.1	54.4	64.3	66.5
T_c	76.8	132.6	151.2	154.7
SU(2)+Higgs+fermions ($m_{\text{top}} = 175$ GeV)				
m_H	–	51.2	68.0	69.4
T_c	–	89.8	105.8	107.2

Table 2

T_c from 4D SU(2)-Higgs simulations.

m_H/GeV	T_c/m_W	N_τ	
16	0.464(2)	3	[12]
34	0.910(16)	∞	[20]
48	1.153(16)	3	[12]

large that the subleading behaviour is seen. Nevertheless, it should be noted that the T^* varies very little across the extrapolation: the curvature is seen only because of the very small statistical errors.

The phase *metastability range* is also shown in Fig. 3. This has been obtained as follows: at y_c , the order parameter histograms have a 2-peak structure. The histograms are reweighted off y_c until the “shoulder” of one of the peaks vanishes; in terms of the constrained effective potential this corresponds to the temperature at which the metastability of the phase vanishes [24].

The 3D effective theory describes a whole class of 4D theories, as discussed in sec. 2.1. In table 1 the physical T_c is shown for 4D SU(2)+Higgs and SU(2)+Higgs+fermions -theories, in addition to the “bare” T_c^* -values. The fermion content is the same as in the MSM, with $m_{\text{top}} = 175$ GeV. Note that the physical m_H is different from m_H^* , and that the $m_H^* = 35$ GeV -set does not correspond to any physical fermion theory.

Locating the critical couplings in 4D simulations is essential for determining CPC, as discussed in sec. 2.2. The methods above can be used

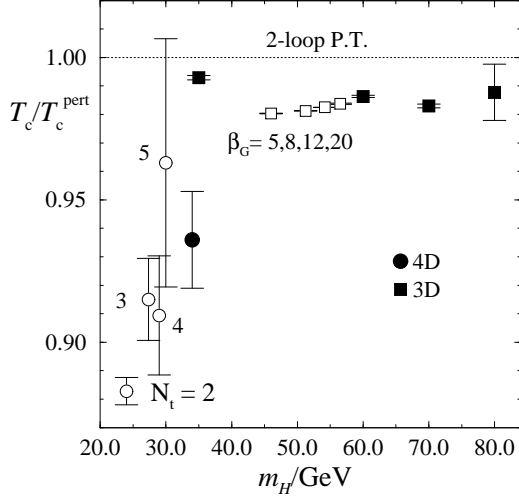


Figure 4. T_c/T_c^{pert} from 4D [20] and 3D [24] simulations. The open symbols show the extrapolation to the continuum limit (only $m_H^* = 60$ for 3D) and have been shifted horizontally for clarity.

also in 4D to locate the critical couplings; in addition the DESY group has used methods which rely on the coexistence of two phases in long cylindrical lattices [12,20]: in the “constrained” method the order parameter is restricted to a narrow range between the pure phase values, enforcing the system to reside in a mixed phase. The coupling is then tuned so that the distribution in this region is horizontal. This is equivalent to the condition that the ‘flat’ part of the 2-peak histogram is horizontal, but requires much less cpu-time than the full histogram calculation. In the “2-coupling” method the system is split into 2 halves, and the critical coupling is bracketed by tuning the couplings in the two subvolumes individually so that the 2-phase configuration is maintained.

In table 2 the ratio T_c/m_W is shown for different m_H . For the 34 GeV case results from $N_\tau = 2$ –5 have been used to extrapolate $a \rightarrow 0$ quadratically.

A direct comparison between 3D and 4D simulations at this stage is not straightforward, due to very different connections to continuum physics. The 3D simulations have used $g^2(7T) \approx 0.444$, whereas in 4D simulations $g_R^2 \approx 0.58$. The re-

lations $(g_3^2, x, y) \leftrightarrow 4\text{D}$ quantities allows one to adjust g^2 ; however, then also the physical m_H changes. Currently there are no simulations which would correspond to the same physical situation (however, see [41]). Nevertheless, it is straightforward to compare the results individually to 2-loop perturbative results. In Fig. 4 T_c/T_c^{pert} is plotted, the squares correspond to 3D $m_H^* = 35, 60, 70$ and 80 GeV cases, circles to 4D $m_H = 34 \text{ GeV}$. Also shown is the approach to the continuum limit; for 3D the points are the same as shown in Fig. 3. A striking feature is the smallness of the statistical errors in the 3D simulations. This is due to the rigorous nature of CPCs in 3D: the errors in T_c are directly translated from the statistical errors of critical couplings. In 4D the errors accumulate through $T = 0$ mass measurements. For the bare values of the critical couplings the accuracy is comparable, up to 6–7 decimal places. The finite a effects are seen to be small in both cases, and T_c/T_c^{pert} is consistently smaller than 1. Given the difference in the values (and renormalization schemas!) of g^2 and the 4D statistical errors the results can not be considered inconsistent.

3.3. Interface tension and latent heat

The tension of the interface σ between the 2 coexisting phases and the latent heat L of the transition are primary quantities characterizing the strength of the transition. The now ubiquitous *histogram method* [42] is the most accurate but numerically very demanding way to measure σ : for each lattice 3-volume $V = a^3 L^2 L_z$, where $L \leq L_z$ is assumed, one measures p_{max} and p_{min} , the probability distribution maximum and the minimum between the peaks at T_c . σ is now obtained at the $V \rightarrow \infty$ limit of the expression

$$\frac{\sigma a^2}{T} = \frac{1}{2L_x^2} \left[\ln \frac{p_{\text{max}}}{p_{\text{min}}} + \frac{1}{2} \ln \frac{L_z^3}{L_x^2} + G + c \right] \quad (18)$$

where $G = \ln 3$ for $L_x = L_z$ and 0 for $L_x \ll L_z$, and c is a constant. In addition, $a \rightarrow 0$ limit should be taken. Eq. (18) has been used both in 3D and 4D simulations [12, 24, 28, 23]. The DESY group [12, 13, 21, 22] has also used the *2-coupling* integration method [43] and the *tunnelling correlation length* [44] analysis. These methods are

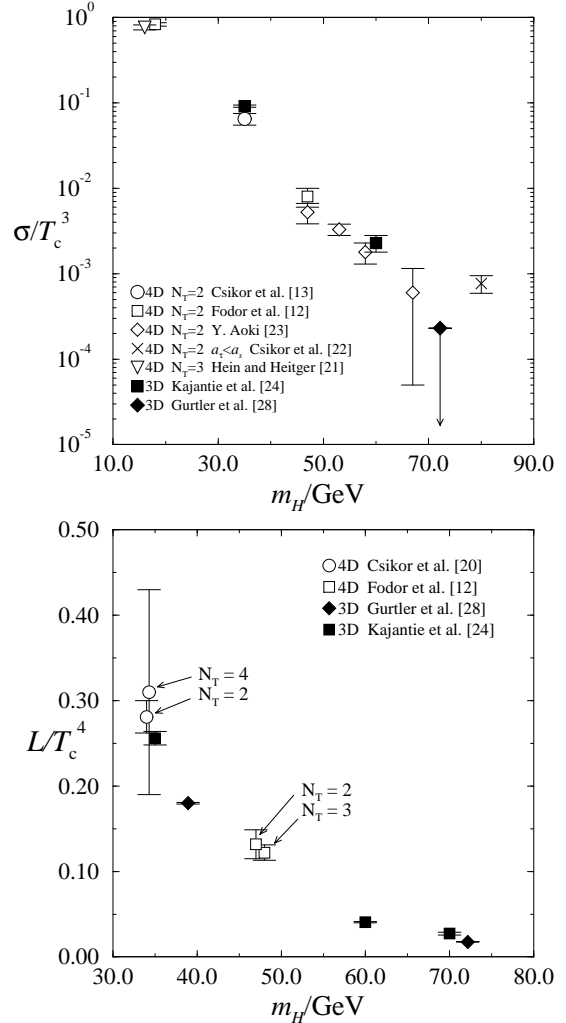


Figure 5. The interface tension (top) and latent heat (bottom) from 4D and 3D simulations.

not quite as demanding computationally as the histogram method.

In Fig. 5 σ is shown from several calculations. Both the 3D calculations shown perform $a \rightarrow 0$ extrapolation. Note the dramatic decrease in σ when m_H increases. Considering the difficulties in measuring σ reliably the agreement must be considered to be good; the only point which disagrees somewhat with the trend is the 80 GeV asymmetric lattice ($a_\tau = a_s/4$, $N_\tau = 2$) point presented in this conference [22]. Perturbatively, σ can be calculated with any reliability only when

the transition is strong: indeed, at very small m_H the agreement between the lattice and perturbative results is fair, but already at ~ 60 GeV the lattice results are a factor of 4–5 smaller.

The latent heat L is directly related to the jump of $\langle\phi^\dagger\phi\rangle$ at the transition through the Clausius-Clapeyron equation:

$$L/T_c^4 = \frac{m_H^2}{T_c^3} \Delta\langle\phi^\dagger\phi\rangle. \quad (19)$$

In Fig. 5 L is shown from 3D and 4D simulations; in 3D the extrapolation to the continuum limit has been performed. Both in 3D and 4D also alternative methods to eq. (19) have been used for measuring L , with practically unchanged results. Within errors, the results are consistent with the 2-loop perturbation theory.

3.4. Interaction measure

The interaction measure $\delta \equiv \epsilon - 3p$ characterizes the deviation of the system from the massless ideal gas behaviour. This has been measured by the DESY group in 4D at $m_H = 34$ GeV [20]; in 3D δ , ϵ and p are not readily accessible. When $0.5 < T/T_c \leq 1$ in the broken phase, $\delta/T^4 \approx 0.6$, and at T_c it jumps discontinuously to ≈ 0.9 . When T increases further δ/T^4 falls rapidly, and at $T \approx 2T_c$ it is ~ 0 . This qualitatively agrees with the perturbation theory in the broken phase, where it is applicable.

4. BROKEN AND SYMMETRIC PHASE

Deep in the broken phase perturbative analysis is well controlled. Lattice studies at $T \lesssim T_c$ can reveal the accuracy and the eventual failure of the perturbation theory. Indeed, as mentioned in the introduction, the expansion parameter is $\sim g_3^2/(\pi m_W)$, where $m_W(v) \rightarrow 0$ formally when the symmetry is restored.

In refs. [24,28] the behaviour of $\langle\phi^\dagger\phi\rangle$ is studied with 3D simulations. The general agreement between the lattice and continuum 2-loop perturbative results is good, progressively becoming worse when T_c is approached. However, since $\langle\phi^\dagger\phi\rangle$ can be determined very accurately in the broken phase (relative error $\sim 10^{-3}$), deviations are seen even relatively deep in the broken phase. This information was used in [24] to infer the value of

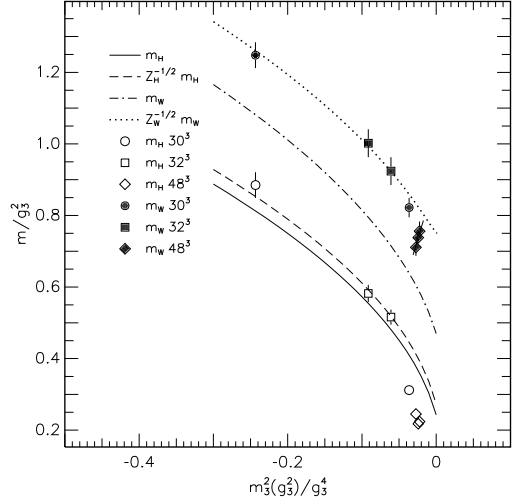


Figure 6. m_H and m_W in the broken phase at $m_H^* = 70$ GeV compared to the perturbation theory (Gürtler et al.[28]).

the so far uncomputed 3-loop term in the effective potential, and to verify that it is linear in ϕ . Even with this correction the effective potential fails at the transition point.

The Higgs and W screening masses are measured with the scalar (0^{++}) and vector (1^{--}) operators of type

$$S_x = \text{Tr} [\Phi_x^\dagger \Phi_x] \quad (20)$$

$$V_{x;i}^a = \text{Tr} [\tau^a \Phi_x^\dagger U_{x;i} \Phi_{x+i}] \quad (21)$$

where τ^a is a Pauli matrix. The masses (inverse correlation lengths) are extracted from the correlation functions $\langle S_x S_y \rangle$ and $\langle V_x V_y \rangle$; in the V -correlations only the diagonal part survives. To improve the signal the operators can be smeared or blocked in various ways.

In Fig. 6 the measured values of m_H and m_W are compared against 1-loop perturbative values (with and without the wave function renormalization) for $m_H^* = 70$ GeV [28]. Deep in the broken phase the results agree within errors; however, closer to the transition deviations appear. Note that perturbatively the transition occurs at $m_3^2 = 0$, whereas in the actual simulations $m_{3,c}^2 < 0$. Similar behaviour has been observed in other simulations [24,26,12].

The symmetric phase vector and scalar masses,

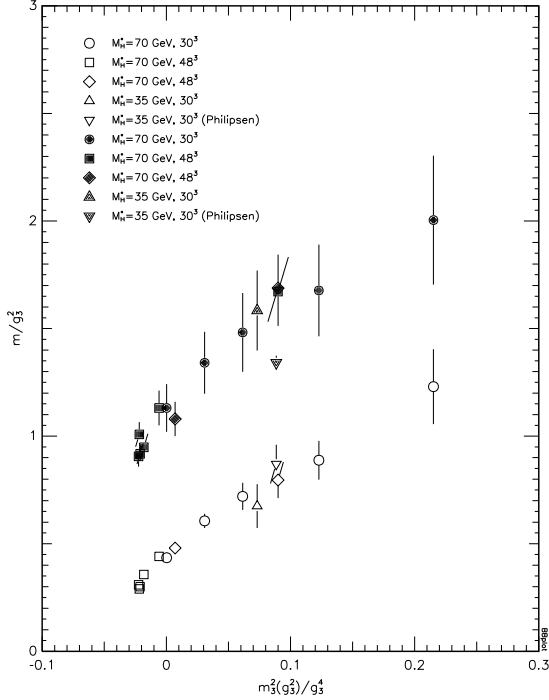


Figure 7. Vector (filled) and scalar (open) masses in the symmetric phase [28].

measured with operators (20-21), are shown in Fig. 7 [28]. Both masses increase when T (m_3^2) increases. An interesting observation is that the $m_H^* = 35$ and 70 GeV masses are equal – this is reasonable, because in the symmetric phase the $\lambda(\phi^\dagger\phi)^2$ -term in the action (3) is very small. Comparing Figs. 6 and 7 we note that there is a small but clearly discernible discontinuity of the masses at the transition: in the symmetric phase the masses become larger. Again, similar behaviour has been observed by other groups [24,26].

Philipsen et al.[29] used various levels of blocking of the operators (20-21), and measured the full correlation matrix between different blocking levels. By performing an eigenstate analysis the ground state and a few lowest excited states could be distinguished. The ground states in the vector and scalar channels are shown in Fig. 7 with downwards pointing triangles. In the scalar channel the mass agrees with the measurements of [28], but the vector mass is slightly smaller,

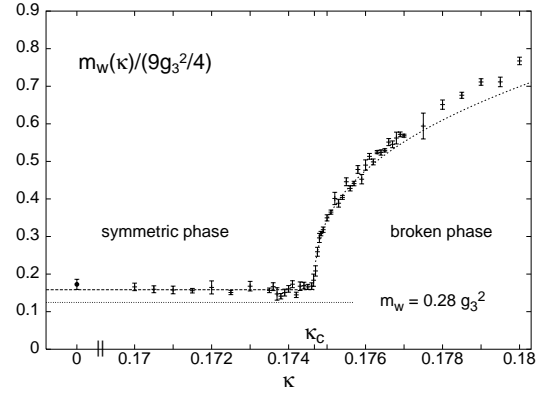


Figure 8. m_W in the Landau gauge (after [26]).

likely due to the better projection to the ground state. In the scalar channel also standard plaquette ‘ W -ball’ operators are used together with the blocked S -operators. In the symmetric phase very little mixing is seen between these operators; furthermore, the masses in the W -ball sector are observed to be almost identical to the 3D $SU(2)$ 0^{++} glueball masses measured at the same value of β_G [45].

In [26] m_W was measured by fixing to the Landau gauge and using A_i^a -operators to measure the correlations. The results are shown in Fig. 8: in the broken phase, the results are equal to those measured with the operators of type eq. (21). However, in the symmetric phase $m_W \approx 0.35g_3^2$, independent of m_3^2 (and T), in strong contrast to the V -operator in Fig. 7. The point at $\kappa = 0$ in Fig. 8 is a pure gauge result, i.e. calculated without the Higgs field.

Can one understand this behaviour analytically? In the symmetric phase the perturbative expansion breaks down. The system may essentially behave like 2+1D $SU(2)$ gauge theory at $T = 0$, which is confining. The Higgs field can be interpreted as a scalar quark, and the physical states are now W -balls and $(\phi^\dagger\phi)$ bound states. Using this strong coupling picture and the static ϕ - ϕ potential determined with lattice simulations [16], Dosch et al.[46] calculated the mass spectrum of the bound states analytically, reproducing the pattern in Fig. 7 quite well. On the other hand, the 1-loop Schwinger-Dyson gap equation calculation by Buchmüller and Philipsen

[38] gives an approximate result $m_W \approx 0.28 g_3^2$ in the symmetric phase. This is obviously in conflict with the vector masses in Fig. 7, but is close to the Landau gauge fixed result, and is shown as a horizontal dashed line in Fig. 8.

The static potential and the string tension σ in the symmetric phase have been measured in [16,28]. Also in this case no significant dependence of σ/g_3^4 on λ (m_H^*) was observed. When $m_3^2(T)$ is large, the value of σ was close to the pure 3D SU(2) gauge theory value [45]. At large distances one expects the screening behaviour to set in; however, this has not been observed yet in the distances presently allowed by the available resources.

These results, while clearly supporting the confinement picture in the symmetric phase, also show that the gauge degrees of freedom decouple almost completely from the Higgs field. Indeed, all the measurements which involve only gauge fields (plaquette correlators, Landau gauge A_i^a correlator, string tension) give results almost identical to the pure SU(2) gauge theory.

5. SPHALERON TRANSITION RATE

Due to the axial anomaly the baryon number is not conserved in the EW theory. In order to quantify the effects of the EW physics to the baryon number of the Universe [2] the knowledge of the sphaleron transition rate Γ is essential. In terms of the gauge fields, Γ is the diffusion rate of the topological charge $B(t) = \Delta N_{CS}(t)$ where N_{CS} is the Chern-Simons number. The effective potential is periodic to the N_{CS} -direction: there are large gauge transformations which change N_{CS} by unity. The goal is to calculate the rate of the dynamical processes which change N_{CS} , driving the configuration from one minimum to a neighbouring one. Since $B(t)$ can be described as a random walk in the periodic potential,

$$\langle B^2(t) \rangle_T \rightarrow \Gamma V t, \quad t \rightarrow \infty \quad (22)$$

where $\langle \cdot \rangle_T$ is the canonical expectation value [47]. From analytical considerations [48] one expects $\Gamma = \kappa(\alpha_W T)^4$, where

$$\begin{aligned} \kappa &= \text{const.} & T > T_c \\ \kappa &\approx f \exp[-E_{\text{sph}}(T)/T] & T < T_c \end{aligned} \quad (23)$$

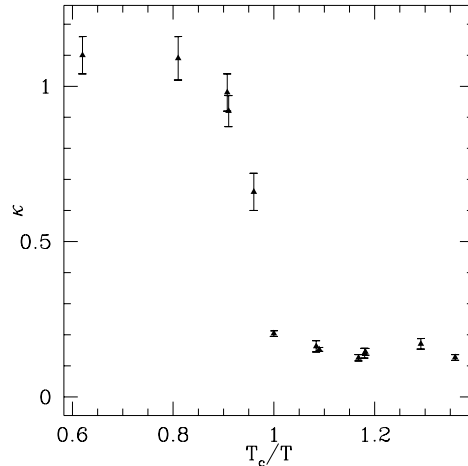


Figure 9. $\Gamma/(\alpha_W T)^4$ for SU(2)-Higgs [30].

The calculation of Γ is non-perturbative. Since Γ is a real-time transition rate, the standard imaginary time lattice formalism is not easily applicable. However, one expects that at high T the transitions occur predominantly through thermally activated classical processes. This suggests the following strategy: $B(t)$ is calculated by solving the *classical* equations of motion, and the results are averaged over a canonical ensemble [49]. It is important that the Gauss constraint is satisfied. This is simple in the 1+1D U(1)-Higgs model, which has been studied in detail as a prototype model [19,50], but for 3+1D SU(2) correct methods have been derived only recently [51,52].

In the 1+1D U(1)-Higgs model the numerical and analytical results agree (however, in the high T phase some lattice spacing dependence remains, see [53]). Ambjørn and Krasnitz [54] measured Γ in the high T phase of the pure gauge SU(2) theory, with the result $\Gamma = \kappa(\alpha_W T)^4$, $\kappa = 1.09 \pm 0.04$. The result was seen to be independent of (large) V and (small) a , indicating that it survives to the continuum limit. This is supported by the result by Moore [52], who also measured the linear response Γ_μ of N_{CS} to a chemical potential, $\Gamma_\mu = 2\Gamma$.

In the 3+1D SU(2)-Higgs model it has been analytically estimated that $\kappa \approx 0.01$ in the high T phase [55]. Tang and Smit have recently calcu-

lated Γ in this model [30]; the results are shown in Fig. 9. In the high T phase $\kappa \approx 1$, which agrees with the SU(2) result but is in strong contrast to the analytical estimate. At T_c κ decreases sharply, and remains 0.1–0.2 when $T < T_c$. The disagreement with the analytic form in eq. (23) is dramatic: no exponential suppression is seen, and the rate is 10^3 – 10^8 times larger than expected! Similar behaviour has been observed by Ambjørn and Krasnitz [56]. The success of the 1+1D U(1)-Higgs model makes this conflict even more striking, and obviously the reason for this must be understood before we can have trust in the results.

6. CONCLUSIONS

The numerical EW simulations have been very successful: to a large extent, the static thermodynamic properties of the EW phase transition have been “solved”. The transition is strongly 1st order at small m_H , becomes rapidly weaker with increasing m_H and at $m_H \approx 80$ GeV (for SU(2)-Higgs) the line of transition ends at a critical point, after which only a smooth cross-over remains. For practical purposes, the accuracy is good enough for most of the static quantities relevant to the transition. The properties of the critical point itself (exact location, exponents) are not yet so well known, this being arguably the most difficult point in the phase diagram. These results rule out the MSM baryogenesis: it is not any more possible that the transition is strong enough to produce the observed B asymmetry [24].

The 2-loop perturbation theory yields a good guideline for the transition at $m_H \leq 70$ GeV, although deviations are clearly seen. The 3D effective theories and their accuracy are now fully understood theoretically, and the good general agreement with the 4D simulations is very encouraging. However, more comparisons should be done in order to fully quantify the accuracy: this is especially important since the 3D theory provides a method for investigating realistic EW (+ beyond) theories without any of the problems usually caused by fermions, chiral or not.

There are still unanswered questions with the current results, which must be addressed: the role

of the different correlation lengths in the symmetric phase is still not fully clarified, and the contradiction between the analytical and numerical results for the sphaleron rate must be understood.

Acknowledgement

Discussions with K. Kajantie, M. Laine, M. Shaposhnikov, K. Jansen, Z. Fodor, K. Jansen, T. Neuhaus and O. Philipsen are gratefully acknowledged. This work has been partly supported by the DOE grant FG02-91ER40661.

REFERENCES

1. D. A. Kirzhnits and A. D. Linde, *Ann. Phys.* **101** (1976) 195; *Phys. Lett.* **72B** (1972) 471.
2. V. A. Kuzmin, V. A. Rubakov, M. E. Shaposhnikov, *Phys. Lett.* **B155** (1985) 36; A. G. Cohen, D. B. Kaplan, A. E. Nelson, *Ann. Rev. Nuc. Part. Sci.* **43** (1993) 27; M. Shaposhnikov, G. Farrar, *Phys. Rev.* **D50** (1994) 774.
3. P. Arnold, O. Espinosa, *Phys. Rev.* **D47** (1993) 3546; Z. Fodor, A. Hebecker, *Nucl. Phys.* **B432** (1994) 127; W. Buchmüller, Z. Fodor, A. Hebecker, *Nucl. Phys.* **B447** (1995) 317.
4. K. Farakos, K. Kajantie, K. Rummukainen and M. Shaposhnikov, *Nucl. Phys.* **B425** (1994) 67; *Nucl. Phys. B* 442 (1995) 317.
5. A. D. Linde, *Phys. Lett.* **96B** (1980) 289; D. Gross, R. Pisarski and L. Yaffe, *Rev. Mod. Phys.* **53** (1981) 43.
6. P. H. Damgaard and U. M. Heller, *Phys. Lett.* **B164** (1985) 121; *Nucl. Phys.* **B294** (1987) 253; *Nucl. Phys.* **B304** (1988) 63.
7. H. G. Evertz, J. Jersák and K. Kanaya, *Nucl. Phys.* **B285** (1987) 229.
8. B. Bunk, E.-M. Ilgenfritz, J. Kripfganz and A. Schiller, *Phys. Lett.* **B284** (1992) 371; *Nucl. Phys.* **B403** (1993) 453.
9. K. Kajantie, K. Rummukainen and M. Shaposhnikov, *Nucl. Phys.* **B407** (1993) 356.
10. K. Kajantie, M. Laine, K. Rummukainen and M. Shaposhnikov, *Nucl. Phys.* **B458** (1996) 90.
11. F. Csikor, Z. Fodor, J. Hein, A. Jaster, I. Montvay, *Phys. Lett.* **B334** (1994) 405.

12. Z. Fodor, J. Hein, K. Jansen, A. Jaster, I. Montvay, Nucl. Phys. **B439** (1995) 147.
13. F. Csikor, Z. Fodor, J. Hein, J. Heitger, Phys. Lett. **B357** (1995) 156.
14. K. Farakos, K. Kajantie, K. Rummukainen and M. Shaposhnikov, Phys. Lett. **B336** (1994) 494.
15. K. Farakos, K. Kajantie, M. Laine, K. Rummukainen and M. Shaposhnikov, Nucl. Phys. **B** (Proc. Suppl.) 47 (1996) 705.
16. E.-M. Ilgenfritz, J. Kripfganz, H. Perlt and A. Schiller, Phys. Lett. **B356** (1995) 561.
17. K. Jansen, Nucl. Phys. B (Proc. Suppl.) 47 (1996) 196.
18. K. Kajantie, Nucl. Phys. B (Proc. Suppl.) 42 (1995) 103.
19. M. Shaposhnikov, Nucl. Phys. B (Proc. Suppl.) 26 (1992) 78.
20. F. Csikor, Z. Fodor, J. Hein, A. Jaster, I. Montvay, DESY 95-206 (hep-lat/9601016).
21. J. Hein, J. Heitger, DESY 96-066 (hep-lat/9605009).
22. F. Csikor, Z. Fodor and J. Heitger, these proceedings.
23. Y. Aoki, these proceedings (hep-lat/9608061).
24. K. Kajantie, M. Laine, K. Rummukainen and M. Shaposhnikov, Nucl. Phys. **B466** (1996) 189.
25. K. Kajantie, M. Laine, K. Rummukainen and M. Shaposhnikov, CERN-TH-96-126, hep-ph/9605288.
26. F. Karsch, T. Neuhaus, A. Patkós, J. Rank, BI-TP-96-10 (hep-lat/9603004).
27. F. Karsch, T. Neuhaus, A. Patkós, J. Rank, these proceedings.
28. M. Gürtler, E.-M. Ilgenfritz, J. Kripfganz, H. Perlt, A. Schiller, hep-lat/9512022; HUB-IEB-96/18 (hep-lat/960542); and these proceedings.
29. O. Philipsen, M. Teper, H. Wittig, Nucl. Phys. **B469** (1996) 445, and these proceedings (hep-lat/9608067).
30. W. H. Tang and J. Smit, hep-lat/9605016, and these proceedings.
31. P. Ginsparg, Nucl. Phys. **B170** (1980) 388; T. Appelquist and R. Pisarski, Phys. Rev. **D23** (1981) 2305; S. Nadkarni, Phys. Rev. **D27** (1983) 388; N. P. Landsman, Nucl. Phys. **B322** (1989) 498.
32. M. Laine, Nucl. Phys. **B451** (1995) 484.
33. F. Karsch, T. Neuhaus, A. Patkós, Nucl. Phys. **B441** (1995) 629.
34. A. Jakovác, Phys. Rev. **D53** (1996) 4538; U. Kerres, G. Mack and G. Palma, Nucl. Phys. **B467** (1996) 510.
35. M. Laine, hep-ph/9605283; J. Cline and K. Kainulainen, hep-ph/9605235; M. Losada, hep-ph/9605266.
36. F. Csikor, Z. Fodor, CERN-TH/96-57 (hep-lat/960302).
37. E. Fradkin and S. H. Shenker, Phys. Rev. **D49** (1979) 3682.
38. W. Buchmüller and O. Philipsen, Nucl. Phys. B 443 (1995) 47.
39. P. Arnold and L. G. Yaffe, Phys. Rev. **D49** (1994) 3003.
40. M. Karjalainen and J. Peisa, hep-lat/9607023; M. Karjalainen, M. Laine and J. Peisa, these proceedings.
41. M. Laine, hep-lat/9604011.
42. K. Binder, Phys. Rev. **A25** (1982) 1699.
43. J. Potvin, C. Rebbi, Phys. Rev. Lett. **62** (1989) 1379.
44. K. Jansen et al., Phys. Lett. **B213** (1988) 203.
45. M. Teper, Phys. Lett. **B289** (1992) 115; **B311** (1993) 223.
46. H.-G. Dosch, J. Kripfganz, A. Laser and M. Schmidt, Phys. Lett. **B365** (1995) 213.
47. S.Yu. Khlebnikov and M.E. Shaposhnikov, Nucl. Phys. **B308** (1988) 885.
48. P. Arnold and L. McLerran, Phys. Rev. **D36** (1987) 581.
49. D.Yu. Grigoriev, V.A. Rubakov and M.E. Shaposhnikov, Nucl. Phys. **B326** (1989) 737.
50. A. Bochkarev, in proceedings of the NATO advanced workshop on electroweak physics, *Sintra Electroweak 1994* 333.
51. A. Krasnitz, Nucl. Phys. **B455** (1995) 320.
52. G. Moore, hep-ph/9603384.
53. J. Smit and W.H. Tang, Nucl. Phys. B (Proc. Suppl.) 42 (1995) 590.
54. J. Ambjørn and A. Krasnitz, Phys. Lett. **B362** (1995) 97.
55. O. Philipsen, Phys. Lett. **B358** (1995) 210.
56. A. Krasnitz, private communication.